BAT Slew Suvey (BATSS): Slew data imaging for *Swift*-BAT

A. Copete, J. Grindlay, J. Hong

April 2, 2009

Abstract

The development of a survey that exploits the event-by-event data capture capabilities of the *Swift*-BAT during periods of spacecraft slewing is instrumental in expanding the overall capabilities of the *Swift* mission by expanding its spatial and time coverage without affecting any of its conventional pointing-mode operations. We hereby demonstrate both the importance and the feasibility of a BAT Slew Survey (BATSS), by first showing that the imaging method employed not only extends coverage but also deepens the instrument sensitivity when compared to pointing observations of equivalent source exposure time and coding fraction. An imaging and detection algorithm for slew-mode data has been devised and implemented for real-time data taking, and the automated pipeline has been shown to handle the required data rates and is capable of reporting positions of candidate GRBs in as short as 2.5 hours for the fastest speeds of spacecraft telemetry downlink. The BATSS system is also equipped to identify candidate transient sources by performing detection across multiple slews, and in addition it monitors the activity of known transients in the nominal BAT energy band of 15-150 keV.

1 Introduction

Conceived as a multi-wavelength observatory for the study of gamma-ray bursts (GRBs) as its primary science, *Swift* (Gehrels et al., 2004) has a nominal mode of operation that requires pointed observation of targets (hereafter referred to as "pointing mode"), given the presence of two narrow-field instruments (NFIs), the X-ray Telescope (XRT, 0.3-10 keV, 23.6 arcmin FOV) and the UV/Optical Telescope (UVOT, 170-650 nm, 17 arcmin FOV) (Swift Science Center, 2008). The third instrument, the Burst Alert Telescope (BAT, 15-150 keV) (Barthelmy et al., 2005), is on the other hand a wide-field (100×60 deg FOV), coded aperture telescope that detects the prompt emission from GRBs and is equipped to

capture photon-by-photon data during slew maneuvers to *Swift* targets. Hence, the BAT provides the possibility of developing a survey that analyzes "slew mode" observations and thus enhances the capabilities of *Swift* by widening its spatial and time coverage, an untapped opportunity before the development of BATSS. Despite the short durations of *Swift* slews and the technical challenge of developing a dedicated system to image and analyze slew data, the enhanced sky coverage and sensitivity that, as will be shown, are inherent to slew observations compared to equivalent pointing observations, make BATSS a window for new *Swift* science that does not interfere with the mission observing program.

2 Motivation for BATSS

The technical justification for BATSS rests on two inherent features of slew observations: one is their predicted ability to span major parts of the sky in a short period of time, both in terms of area and frequency of coverage, and a quantitative analysis of this property is presented in the remainder of this section based on studies of *Swift* attitude data. The second is an increased sensitivity relative to pointings of equal exposure, which is attributed to the effect of scanning the detector plane across the sky that translates effectively into a measurable reduction of systematic effects. BATSS sensitivity measurements are the subject of section 4, since they first require an understanding of the BATSS imaging procedure and its associated systematics. Combined, these properties of BAT slew observations favor an increment in the detection probabilities for astrophysical sources such as GRBs and fast transients, and simulation work done to predict such probabilities, as well as estimates of BATSS trigger rates along with summaries of confirmed detections to date, are presented in forthcoming papers on BATSS science results.

BATSS sky coverage is a function of the orbital properties and observing strategy of *Swift*. The spacecraft flies in a low-Earth ($\sim$600 km) orbit, with an orbital period of approximately 95 minutes, and is subject to several Sun-Moon-Earth observing constraints (Swift Science Center, 2008). Therefore, it does not have a continuous viewing zone in pointing mode and must slew between targets $\sim$4 times per orbit, with a maximum slewing speed of 1 arcmin/sec. Fig. 1 illustrates the corresponding spacecraft attitude for a typical day's worth of observations (11/08/08), with slews represented as tracks drawn by the center of the BAT FoV, along with a plot of slewing speeds over the course of the same day. In turn, the BAT instrument covers an area of 100×60 deg (1.4 sr, half-coded) around each attitude position, and the resulting total daily sky exposures in pointing and slew modes are also shown in Fig. 1.

In order to draw an absolute comparison of sky coverages in slew vs. pointing mode as a function of time, we have computed the cumulative percentages of covered sky over the course of a typical day (10/29/08) and shown the results in Fig. 2. The calculation assumes continuous coverage in both observing modes, except for periods of SAA passage, and includes all portions of the sky above 1% partial coding in the BAT field-of-view.

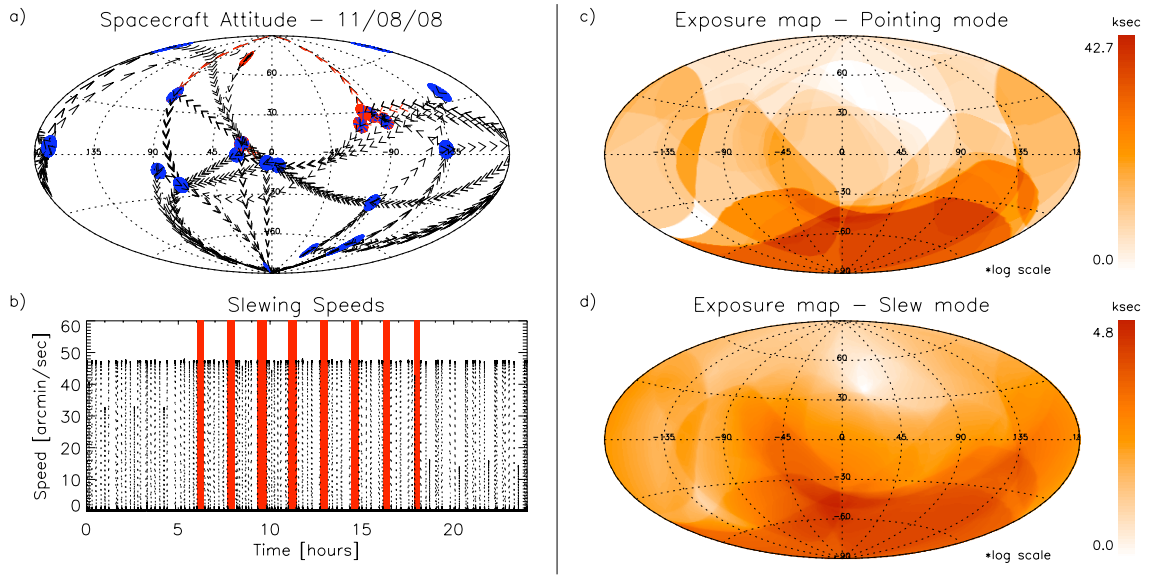

Figure 1: a)*Swift* attitude for a typical day (11/08/08): pointing mode locations (galactic coordinates) are shown a blue dots, along with slew-mode trajectories shown as strings of black arrows. Attitude records taken over the SAA are shown in red, and disregarded from subsequent analysis. b)Plot of slewing speeds, illustrating the typical daily frequency of slew maneuvers and maximum speeds achieved. Periods of SAA passage are highlighted in red. c,d)Maps of corresponding absolute daily exposures of the BAT instrument, in pointing and slew modes respectively.

Furthermore, the curves have been smoothed by averaging over the starting time of the cumulative distribution. The result is a distribution that shows a consistent advantage for the slew-mode coverage over the course of a day, despite a difference in total exposure time of 17.97 hr in pointing mode vs. 2.63 hr in slew mode.

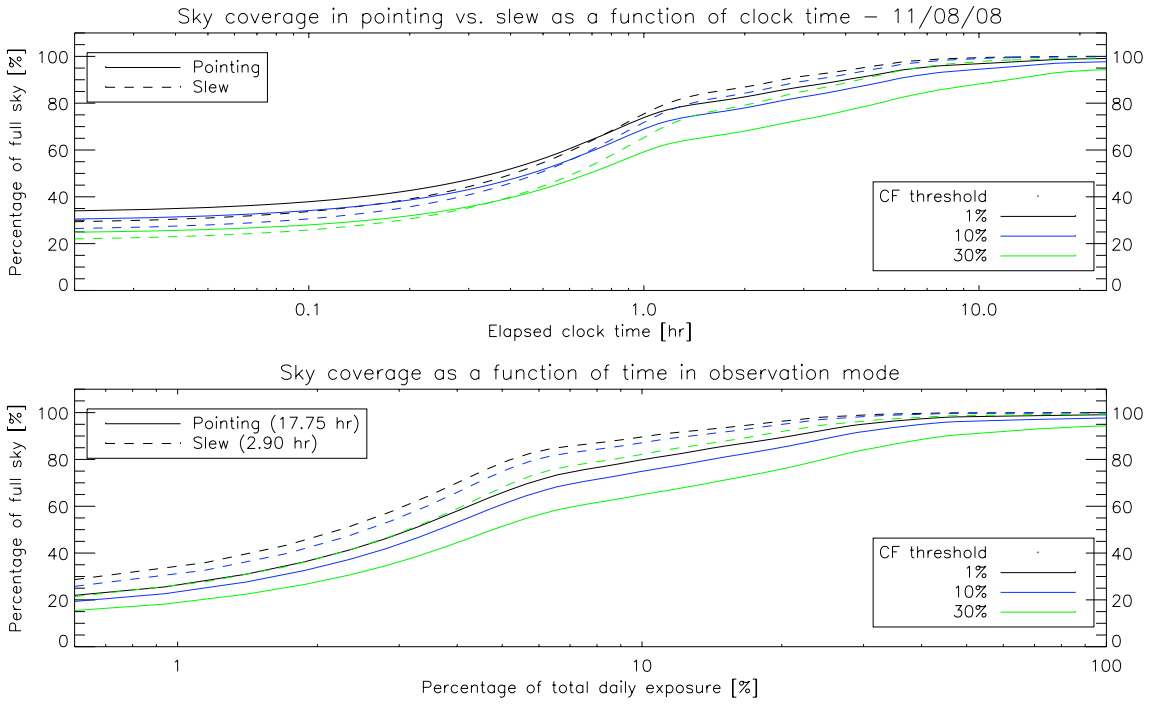

Figure 2: BATSS cumulative sky coverage in comparison with pointing-mode coverage, down to a 1% partial coding threshold, plotted as a function of percentage of the total daily exposure for each observation mode, for a typical day's worth of observations (10/29/08).

3 BATSS imaging and detection algorithm

While taking data during a pointing, the BAT will normally operate in "survey" mode (Barthelmy et al., 2005), wherein photon events are accumulated as Detector Plane Histograms (DPH), which are 3-dimensional arrays of counts across the 286×173 pixels of the BAT detector plane (including gaps between detector modules) and 18 energy bins, taken in 5-minute time bins. Given the fixed attitude, pointing DPHs can be readily correlated with the BAT coded mask pattern to yield sky images in different energy ranges. By contrast, slew observations require imaging over short time intervals of approximately constant attitude, which in turn requires a fine time resolution of input photon events unlike that provided by survey-mode data. Hence, BATSS observations require input data

in BAT's "event" mode, wherein event-by-event data is provided with a time resolution of 0.1 ms. BATSS imaging is based on producing full-sky images out of this input event-mode data over several energy bands, followed by a detection phase based on triggering on these images while requiring coincident detection across energy bands, and the processing algorithm developed for this purpose is described in this section.

3.1 Imaging algorithm

The BATSS imaging algorithm, summarized in the diagram in Fig. 3, can be divided into three major phases: a first phase that implements the coded aperture imaging technique, from accumulation of events in the BAT detector plane to correlation with the coded mask to produce sky images, while relying on the use of the dedicated BAT software package (Markwardt et al., 2007) to handle peculiarities of the BAT instrument. The second phase implements projection of images onto the BATSS full-sky projection, which was developed to allow for imaging and detection in the large fields-of-view that are characteristic of BATSS images, while the third phase performs addition of the projected images to produce a final set of images per slew.

3.1.1 Coded aperture imaging

As a first step in the imaging of a given slew, the input event-mode data is accumulated into Detector Plane Images (DPIs), though the use of the standard BAT software tool **batbinevt**[1], for every 0.2 sec time bin, in 2 independent energy bands: 15-50 keV (hereafter called the "soft band") and 50-150 keV (hereafter called the "hard band"). The 0.2-sec imaging rate is the same rate at which spacecraft attitude data records are taken, and it takes into account the maximum spacecraft slewing speed of 1 arcmin/sec, which would produce a maximum systematic distortion of the slew image PSF of 0.2 arcmin, or 0.9% of the BAT instrument PSF of 22 arcmin (FWHM), and is a second-order effect compared to the systematic source locatization error of $\gtrsim 3$ arcmin in pointing mode (Swift Science Center, 2008) as well as in slew mode, as shown in section **??**. Now, given that DPIs lack information on hot/cold/disabled detector pixels that must be screened from the imaging phase, it is necessary at the same time to create a detector quality map for the entire slew. Given the low number of counts on each of the 0.2-sec DPIs, a single DPI is created from all the events in the 15-150 keV energy range accumulated over the course of the slew, only for the purposes of screening pixels with unusually high/low count rates. The standard BAT software routine **bathotpix** performs the final screening, taking also as input the map of known enabled/disabled pixels that is regularly telemetered along with the input event data.

The next imaging step involves the creation of 0.2-sec sky images and variance maps by cross-correlation with the BAT coded mask, given the input DPIs, detector quality map,

[1]See Markwardt et al. (2007) for a complete description of the BAT software package

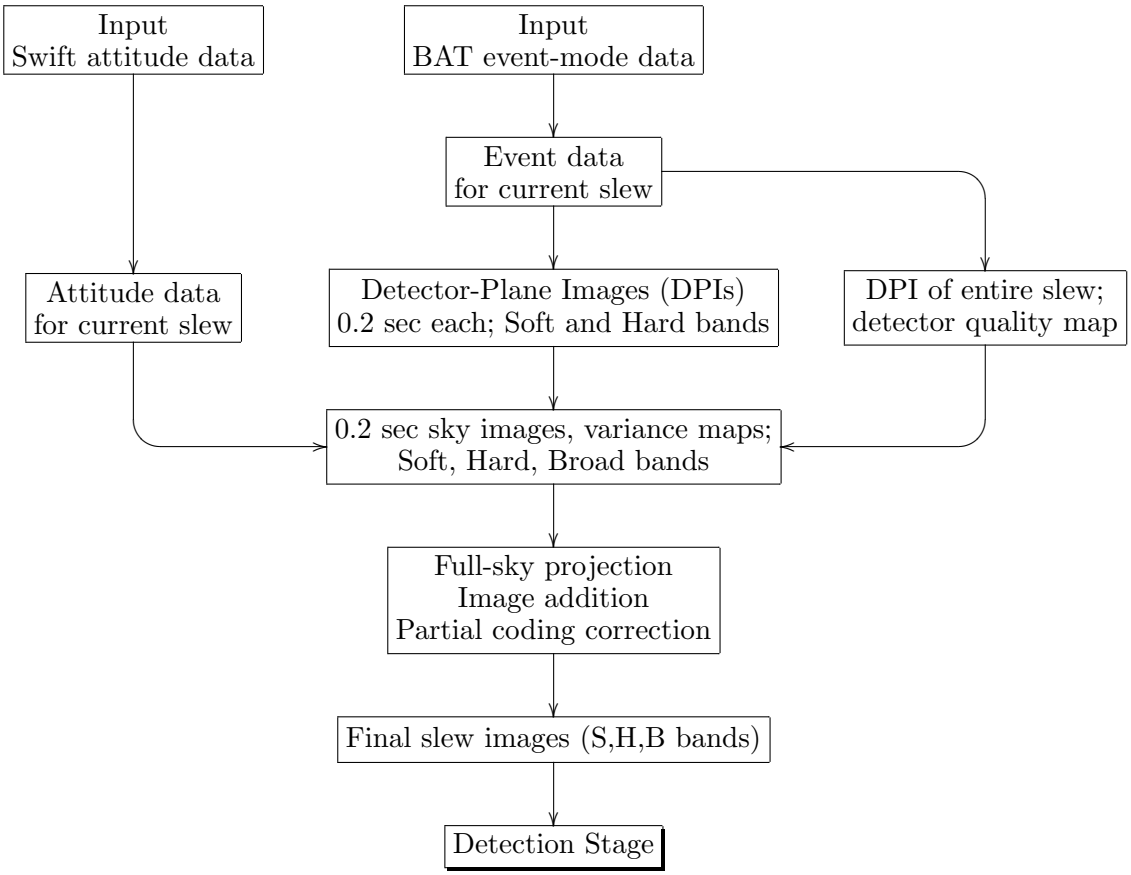

Figure 3: Flow chart of BATSS imaging algorithm

and attitude data for the slew, with the FFT operation performed by the BAT software tool **batfftimage**. All standard corrections for geometrical effects are performed except for the correction for partial coding, which is done only after a co-added slew image has been obtained. Following this, sky images for the 15-150 keV energy band (hereafter called the "broad band") are produced by co-adding the corresponding 0.2-sec sky images in the soft and hard energy bands, in order to enable image triggering based on any combination of detections in the three energy bands.

3.1.2 Full-sky projection

A particular issue for BATSS concerns the sky projection to be used in co-adding the individual 0.2 sec sky images, each of which having the standard size and D-shaped field-of-view of the BAT, but with the varying astrometry parameters characteristic of slew images. The resulting slew image would span a large field-of-view of several steradians, and for this reason it was necessary to adopt a new standard sky projection for BATSS images.

The standard BATSS projection, shown in Fig. 4, was chosen to be a full-sky projection in galactic coordinates, with a fixed set of astrometry parameters, which readily enables addition of images not only within a slew, but also later across several slews for deeper survey observations. Furthermore, for the new projection not to introduce significant systematic effects at the detection stage, it was necessary for it to be approximately equal-area and conformal (i.e. local axis angles and scales are preserved). The zenithal gnomonic (tangential) projection used in standard BAT images, defined as a function of polar angle θ as $R_\theta = \frac{180^\circ}{\pi} \tan\theta$, was evidently not appropriate for this purpose, however, since it introduces distortions in the shape of the PSF as large as a factor of 2 at $\theta = 45^\circ$ from the center of the projection, and eventually diverges at $\theta = 90^\circ$. Instead, we made use of a projection of the generic type quadrilateralized spherical cube (quad-cube), whereby the celestial sphere is projected onto the 6 faces of an enclosing cube, so every point in the projection lies within a maximum of 55° off the center of a sub-projection.

Now, the sub-classes of quad-cube projections defined for the FITS standard by Calabretta & Greisen (2002) all have the property that the edges of contiguous sub-projections match each other exactly, and at these regions the source PSF may differ significantly from the Gaussian shape that is assumed by the detection routine. In order to avoid these projection edge effects, we have instead extended the field-of-view of each of the 6 sub-projections by 5° from each edge, as illustrated by the shaded areas of Fig. 4. In addition, in order to ensure a uniform solid angle to be subtended by each image pixel (a size of $8' \times 8'$ was chosen to optimize for processing speed), for each sub-projection we have implemented a zenithal equal area (ZEA) projection type, whose parameterization for FITS is specified by Calabretta & Greisen (2002), and is defined as a function of the polar angle θ from the

center of each sub-projection as

$$R_\theta = \frac{180^\circ}{\pi}\sqrt{2(1-\cos\theta)} = \frac{360^\circ}{\pi}\sin\frac{\theta}{2}$$

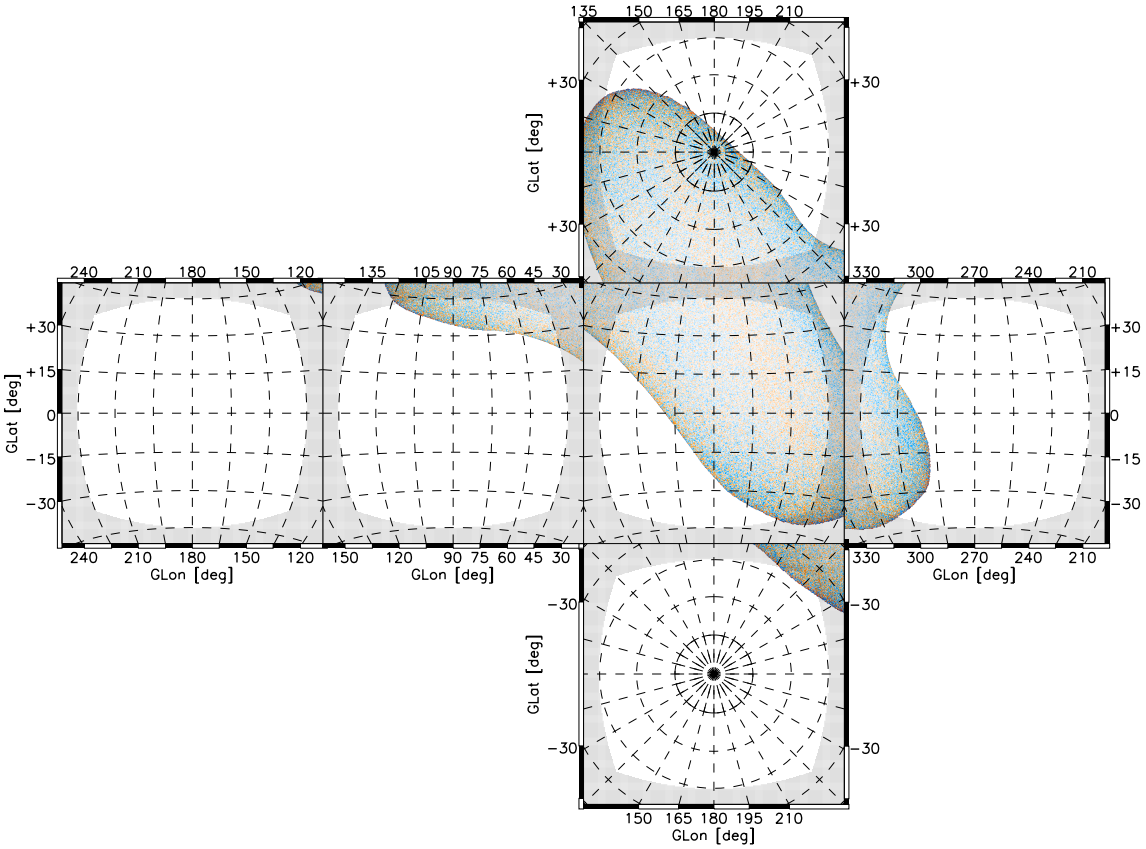

Figure 4: Standard full-sky BATSS projection for slew images: *quad-cube* arrangement with *zenithal equal area* sub-projections. A co-added slew image is shown as an example

The BATSS full-sky projection shown in Fig. 4, where a full slew image is depicted as an example, illustrates several of the features of the model chosen. First, the fact that no pixel in the projection lies further than 54.73° from the center of a sub-projection means that the PSF is distorted by a maximum factor of 0.89 (an 11% reduction) in the radial direction. Compared to a PSF enlargement of 26% at the same distance in BAT-standard gnomonic projection, this means that PSF distortion effects are not only minimized but also improved upon with respect to standard BAT imaging. Second, the addition of a large buffer (shaded) region at the edges of each sub-projection entails that the detection routine can be run independently on each of the sub-projections without any bias due to

the presence of the projection edges. For the probable case of duplicate detections near the edges of adjacent sub-projections, we keep only the detection whose centroid lies within the boundaries of a sub-projection (i.e. outside the buffer region). Finally, once a slew or a portion of a slew has been projected onto the BATSS full-sky projection, it can be readily co-added with any other slew or portion of a slew.

3.1.3 Image addition

Following projection onto the standard BATSS full-sky projection, the individual 0.2-sec images that were obtained from the coded aperture imaging phase are then co-added by variance-weighted addition, producing a single image for the full slew for each of the 3 energy bands, as illustrated in the Fig. 4 example. Given that every sky pixel is swept over by a range of BAT detector coding fractions, it is possible that the low partial coding, less sensitive regions near the edge of the BAT FoV in the 0.2-sec images have an effect on the full co-added image that negatively affects the overall slew sensitivity, thereby raising the question of imposing a threshold in the range of BAT coding fractions that are used in BATSS images. In order to derive such coding fraction threshold, we selected a number of slew observations over the Crab, wherein it goes from outside of the BAT FoV to the fully-coded region over the course of the slew, and co-added the regions of the 0.2-sec images above a pre-set threshold in the range 1% (minimum allowed) to 80% coding, in 5% increments. The results of this test are shown in Fig. 5, where the Crab S/N is plotted against the chosen coding fraction thresholds, from images in 3 energy bands. The results for all observations agree in the monotonic improvement of the sensitivity up to a $\sim$20% threshold level, after which the improvement reaches a plateau and eventually begins to decrease monotonically above $\sim$60%, where the reduced slew exposure time finally outweighs the gains of only co-adding regions of high source coding fraction. From here follows the imposition of a threshold of 15% coding for all 0.2-sec images as they are co-added into a BATSS slew image.

As a final step in the BATSS imaging stage, the image counts are corrected for partial coding, so as to recover the correct source fluxes in the detection stage, by dividing the images by the time-averaged partial coding map for the slew. In slew observations this is the operation that is analogous to the standard partial-coding correction of pointing mode images (Markwardt et al., 2007), whereby the sky image is divided by the BAT partial coding map. The systematic effects of this imaging method on detected sources are described and quantified in Copete et al. (2009).

3.2 Detection algorithm

Taking the co-added slew images in soft, hard, and broad energy bands as input, as well as other auxiliary images, the BATSS detection stage then follows as summarized by the diagram in Fig. 6. The first step involves the use of the BAT standard detection tool

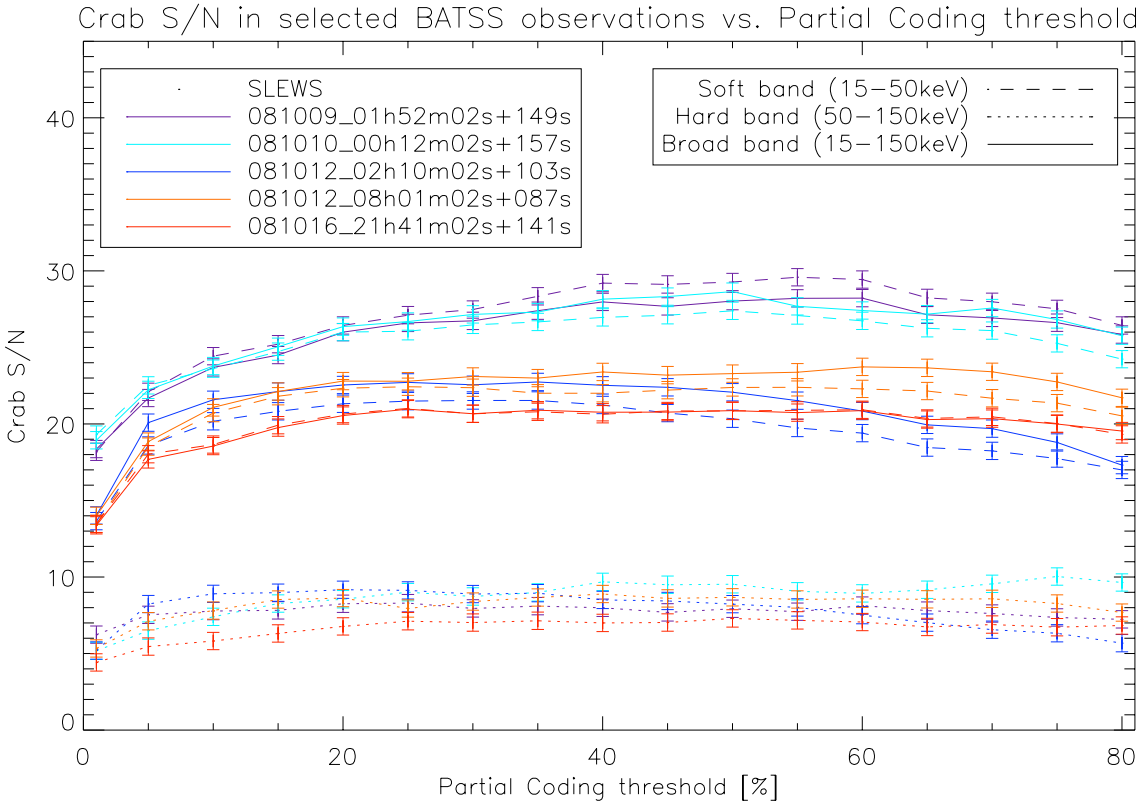

Figure 5: Derivation of coding fraction threshold for BATSS images from selected slew observations over the Crab. The increase of the Crab S/N as a function of coding fraction threshold for each energy band detection is shown as a percentage of the S/N at the minimum threshold level of 1%

batcelldetect, which is called to perform detection on the 3 sky images separately (6 ZEA sub-projections each, as explained in section 3.1.2), using blind detection for uncatalogued sources, and also forcing detection of catalogued sources for monitoring and calibration purposes. As parameterized in BATSS, the blind detection algorithm of **batcelldetect** — further described in Markwardt et al. (2007)— uses a circular sliding cell to find pixels that exceed a pre-set 3.5σ threshold above the background level on the cell, and then on a second pass fits for position and flux by employing a Gaussian PSF of fixed width 22.5 arcmin (FWHM), which corresponds to the BAT instrumental PSF (Swift Science Center, 2008). This produces a catalog of detections which are then sorted according to whether they match a catalog of known transients. Those found to coincide with a catalogued transient are set aside for monitoring of source activity, whereas unidentified detections are further processed for classification as either candidate GRBs or transients.

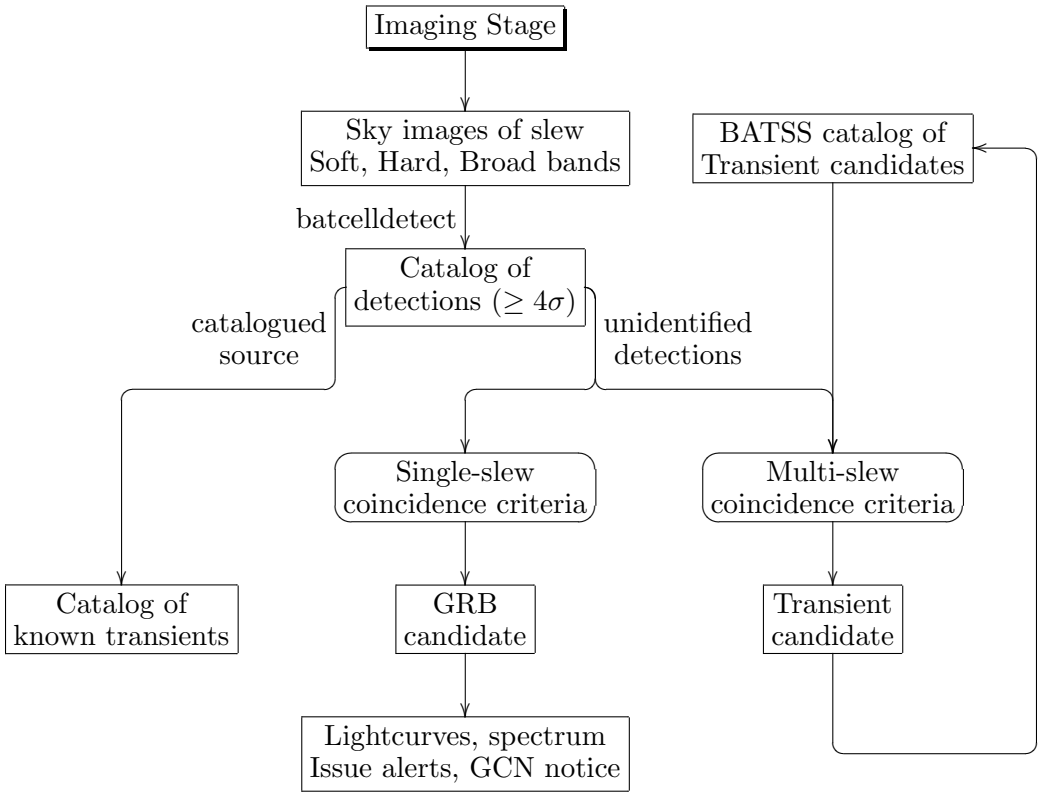

Figure 6: Flow chart of BATSS detection algorithm

Given the likelihood that a number of unidentified detections will correspond to background fluctuations rather than emission from real point sources, the BATSS detection

algorithm additionally employs criteria that require spatial coincidence between several detections in order to categorize them as source candidates. The first set of criteria apply to single-slew (i.e. simultaneous) detections across different energy bands, which give rise to candidate GRBs. These criteria, laid out in detail in section **??**, assign an index number (figure-of-merit) to each candidate according to its likelihood of corresponding to a real GRB. Those with the highest index numbers are in turn subject to further analysis, including derivation of mask-tagged lightcurves and spectra, and generate a set of automated alerts, ending with the issuance of a Gamma-ray bursts Coordinates Network (GCN) Notice that is readily distributed to the world via the GCN Network[2], and in a specific format for BATSS GRB detections[3]. On the other hand, the second set of criteria for candidate source classification employ a multi-slew coincidence scheme that takes the unidentified detections for the current slew and match them against those from all previous slews, in order to identify new candidate transients, particularly repeating ones. Though these candidates do not currently produce world-wide automated alerts, they are kept in an ongoing BATSS catalog of transient candidates for further analysis.

4 BATSS sensitivity

The combined effects of the instrument systematics and imaging methods employed in BATSS observations yield an overall survey sensitivity to point sources that is measurably different from that achieved in pointing observations. In order draw a global empirical comparison of sensitivities in the two observing modes, we have run a month-long survey of bright catalogued sources where we have derived the relative uncertainties in measured fluxes –including all systematic effects– for each day of the survey, scaling for equivalent source exposure times and coding fractions, while also taking into account the discrepancies due to source variability. The slew observation data has been taken from BATSS results over the month of October, 2008, while pointing observation data for the same month has been taken from the Swift/BAT Hard X-ray Transient Monitor[4], which contains results of both single and daily pointing observations on a large number of known transient sources (15-50 keV), with a set of systematic corrections applied to the input data that are standard to BAT pointing data products.

Fig. 7 shows the statistical sample of exposures in both observing modes that were used for this survey, where the sample of observations has been limited to the daily detections of the 15 brightest sources over the full sky. For the purposes of matching the exposure times in pointing and slew modes, we first took into account the nominal exposure time of individual pointing observations, which are taken in intervals of 300 sec up to a average

[2]http://gcn.gsfc.nasa.gov

[3]Notice type **BAT_Slew_Pos** from the complete list of GCN/Swift GRB Notices at http://gcn.gsfc.nasa.gov/swift.html#tc24

[4]Swift/BAT transient monitor results provided by the Swift/BAT team

exposure in the order of 1000 sec, as can be seen from the histogram of orbital exposures. In order to achieve this typical exposure from single slews, where a source gets ∼100 sec of exposure, it is necessary to co-add ∼10 slew images, which is the same order of magnitude of the total slew-mode exposure of a source in a day's worth of observations. Hence, the input slew images chosen for the sensitivity comparison were the co-added daily images for each of the 31 days of the survey, for a total of up to 31 detections per source, each with a net exposure $T_{\rm src} \sim 1000$ sec, as shown in Fig. 7. As for the pointing detection data points, for each day of the survey the daily average measured flux of each source has been used, and the corresponding error values have been scaled for an equivalent exposure of $T_{\rm src}$, assuming a dependence of the statistical error on the exposure time that goes as $1/\sqrt{T}$, as expected from Poisson statistics. At the same time, the statistical errors for both pointing and slew data have been scaled to an equivalent mean coding fraction f of 100%, assuming a dependence of $1/f$ of the statistical error on source coding fraction.

The results of this sensitivity survey are summarized in Fig. 8 for the same 15 bright sources of Fig. 7. The comparison of S/N, in this case defined as the ratio of measured flux to the total error in the measurement (including statistical as well as systematic error), show a consistent advantage in the sensitivity of the slew observations, despite the evident scatter in the plot due in large part to source variability. For this sample, the mean ratio of sensitivities has been found to be 1.91 ± 0.45, a remarkable result given the smaller number of systematic corrections that are regularly applied to the input slew data, and which strongly suggest an inherent advantage to the observational method of scanning the detector plane across the sky compared to fixed attitude in the reduction of systematic effects.

5 Conclusions

Even though the *Swift*-BAT instrument was designed primarily to collect data in an observation mode with fixed spacecraft attitude, we have hereby demonstrated the importance of slew observations in expanding the sky coverage of the BAT, particularly when compared with pointing-mode coverage at short time scales. We have also developed an imaging algorithm for processing the event-by-event data that it is necessary to collected during slew observations and that ultimately produces images in 3 energy bands (15-50 keV, 50-150 keV, 15-150 keV), which are in turn used by the detection algorithm to identify candidate GRBs and Transients, as well as to monitor the activity of known sources.

The BATSS imaging method, along with the intrinsic properties of slew observations, has also been shown to produce images with comparable and even lower systematic effects (uncertainties in source flux and position) than analogous observations in pointing mode. This results in a superior sensitivity in slew mode when comparing with pointings of equivalent source exposure time and coding fraction, which has been demonstrated explicitly in a month-long study of daily slew and pointing observations of 15 bright transient sources,

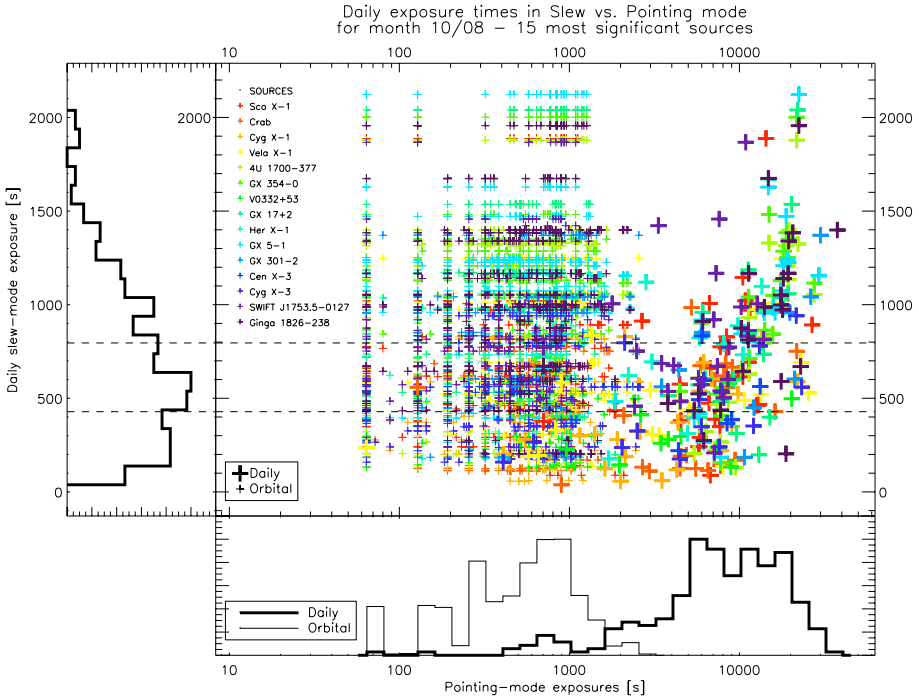

a)

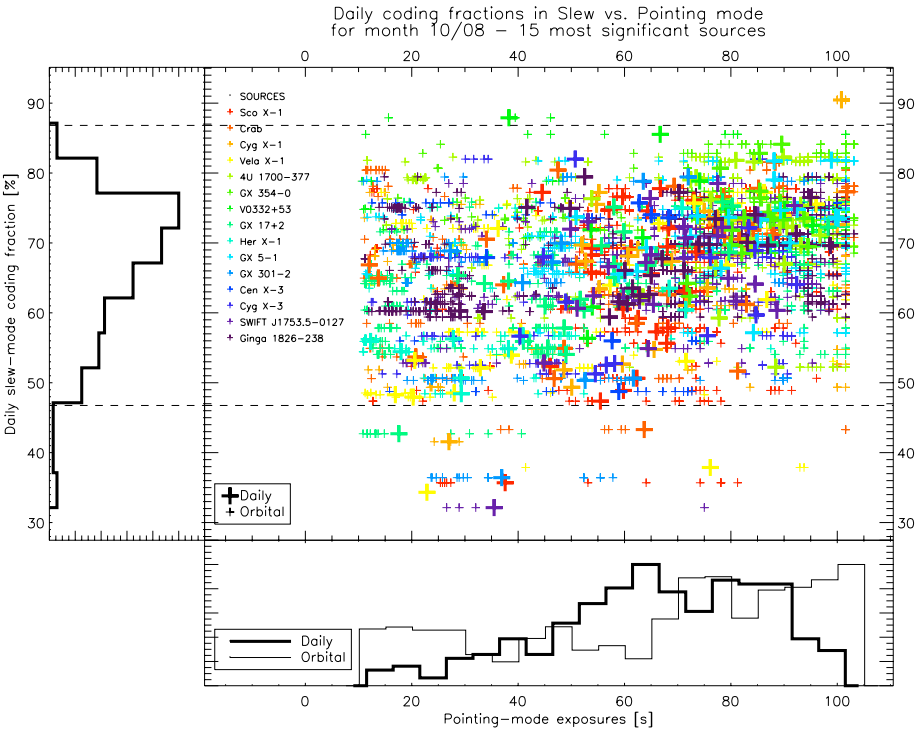

b)

Figure 7: Comparison of actual exposure times (a) and coding fractions (b) in BAT pointing vs. slew mode for 15 bright catalogued sources observed over the period of 1 month (October 2008). For pointing observations, both daily and orbital values are plotted and histogrammed, while only the total corresponding daily values are shown for slew observations.

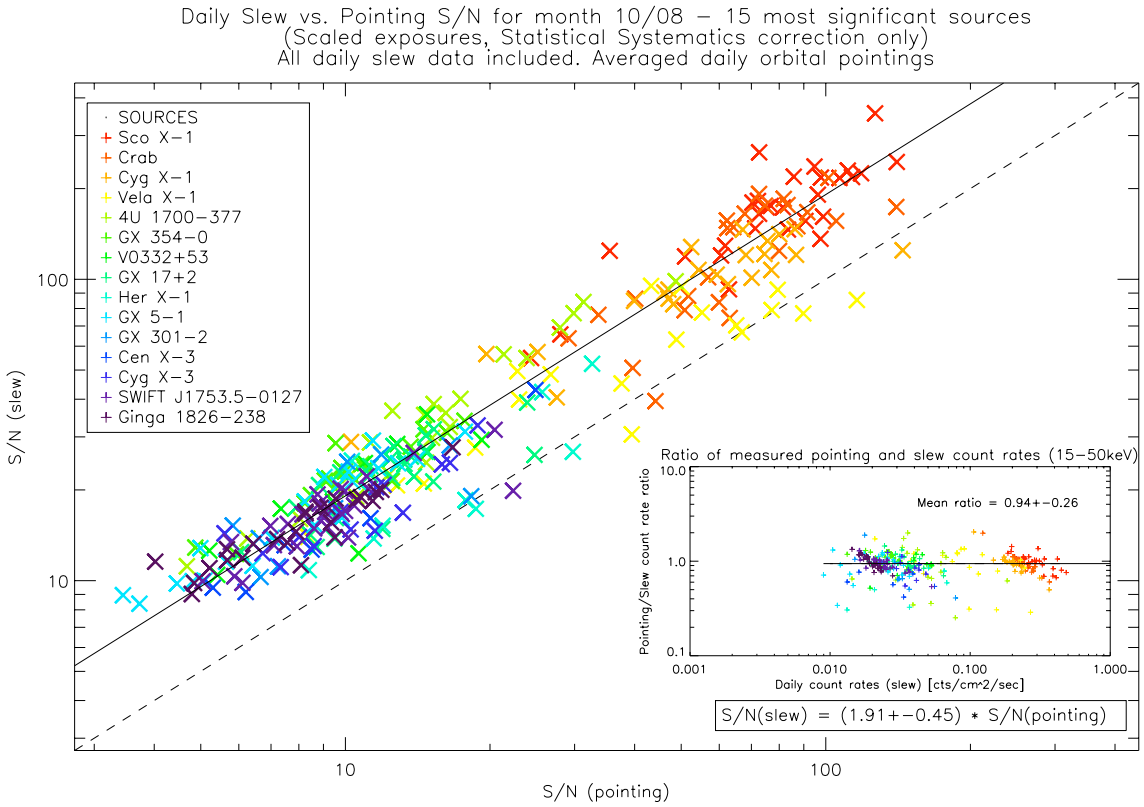

Figure 8: Comparison of sensitivities in pointing vs. BATSS slew observations for 15 bright catalogued sources observed over the period of 1 month (October 2008).

and that resulted on average detection significance that is 2.09 times higher in slew mode.

Finally, we reviewed the actual implementation of the pipeline that is already in place in the BATSS servers, which carries out the imaging and detection algorithms while keeping up with the rate of incoming data, and has been demonstrated to report positions of candidate GRBs –as well as fluxes, lightcurves and spectra– in as little as 2.5 hours from the time of the BAT observation, and longer depending mostly on the speed of the telemetry downlink to the ground station and subsequent transfer to the BATSS machines. Candidate sources from the detection stage have been ranked by index number (figure-of-merit) into 6 types according to their likelihood of corresponding to new real GRBs or Transients. In forthcoming publications we will examine the real vs. expected rates of detection of these candidate types, as well as reporting on the science analysis of BATSS sources that have been confirmed to be real and have been subject to follow-up observations.

References

Barthelmy, S. D. et al.: 2005, *Space Sci. Rev.* **120(3/4)**, 143

Calabretta, M. R. and Greisen, E. W.: 2002, *Astron. Astrophys.* **395**, 1077

Copete, A. et al.: 2009, *BAT Slew Survey (BATSS): Processing Pipeline and Systematics*, in preparation

Gehrels, N. et al.: 2004, *Astrophys. J.* **611**, 1005

Markwardt, C. B. et al.: 2007, *The Swift-BAT Software Guide, v6.3*

Swift Science Center: 2008, *The Swift Technical Handbook, v4.0.1*